Measurement of spin-exchange rate constants between ^{129}Xe and alkali metals

Wenjin Shao, Guodong Wang, and Emlyn W. Hughes
Department of Physics, Division of Physics, Mathematics, and Astronomy, California Institute of Technology, Pasadena, California 91125, USA

(Received 3 September 2004; revised manuscript received 14 February 2005; published 17 August 2005)

By measuring the relaxation rates of the nuclear spin polarization of ^{129}Xe in the presence of alkali-metal vapor at different densities, we have extracted the spin-exchange rates between ^{129}Xe and the three alkali metals K, Rb, and Cs. By studying the alkali-metal–^{129}Xe spin-exchange rates as functions of the cell number density from 0.2 to 0.7 amagat, the binary collision and van der Waals molecular terms are separated, and constants governing both mechanisms are determined. The results from our work can be used to optimize the parameter space for polarizing ^{129}Xe, a promising agent for magnetic resonance imaging and other applications.

DOI: 10.1103/PhysRevA.72.022713 PACS number(s): 34.30.+h, 32.80.Bx, 13.88.+e

I. INTRODUCTION

Techniques for polarizing ^{129}Xe have been developed to achieve ^{129}Xe nuclear polarization on the order of 10% [1,2], about 10^5 times larger than its thermal polarization at room temperature under a magnetic field of 1. The high polarization using weak magnetic fields makes ^{129}Xe a promising agent for numerous applications including medical diagnosis [3,4], surface studies [5,6], and searches for permanent electric dipole moments [7]. Compared to polarizing ^{3}He [8,9], however, the polarization for ^{129}Xe at high densities is still lower by a factor of ~5. Studying ways to improve the ^{129}Xe polarization for high-density applications is an important endeavor.

One of the most widely used approaches for producing hyperpolarized ^{129}Xe is spin-exchange optical pumping [10,11]. Here, circularly polarized laser beams are used to polarize the valence electrons in alkali-metal atoms. The polarized electrons subsequently interact with and polarize the nuclear spin of ^{129}Xe. Currently, Rb is most frequently used for polarizing ^{129}Xe; however, K and Cs are possible alternatives (an example of using Cs to polarize ^{129}Xe is reported in [12]). The spin-exchange process between alkali metals and ^{129}Xe involves both exchange during binary collisions, and exchange by forming alkali-metals–^{129}Xe van der Waals molecules [11,13]. Of them, the latter case requires the presence of a third body. The constants related to both mechanisms are among the most important factors that determine the polarization of ^{129}Xe. Knowledge of these constants, for different alkali metals is valuable for optimizing the ^{129}Xe polarization.

Measurements of the spin-exchange rate constants between the alkali metals K, Rb, and Cs and ^{129}Xe at low cell densities and in N_2-dominated environments have been previously performed by Zeng *et al.* [14]. For current efforts in the production of hyperpolarized ^{129}Xe, higher cell densities (~1 amagat)[1] and Xe-dominated environments are usually used. Accurate measurements of the spin-exchange rate constants for the high-density and Xe-dominating conditions are therefore important, as these conditions are notably different from what have been studied. The constants for ^{129}Xe-Rb spin exchange have more recently been measured by Cates *et al.* at ~1 amagat densities [15], but measurements for ^{129}Xe-K and ^{129}Xe-Cs under similar conditions have not been performed. In this paper we present measurements of the spin-exchange constants between K, Rb, and Cs and ^{129}Xe for cell densities in the range of 0.2–0.7 amagat. Table I presents combinations of alkali-metals–^{129}Xe pairs and experimental conditions. The combinations in which the constants have been measured in existing literature and those in which the constants will be presented in this paper are marked in Table I.

Another issue that has arisen in recent years concerning the determination of the ^{129}Xe spin-exchange rate constants is the applicability of the empirical saturated vapor density formulas for the alkali metals. In the experiments by both Zeng *et al.* [14] and Cates *et al.* [15], these formulas have been applied to calculate the alkali-metal number densities in the cell from the measured cell temperatures; but in several recent papers [16,18], it has been reported that the values from the empirical formulas can vastly differ from the directly measured alkali-metal densities. Some researchers (e.g., [16]) also reported cell-to-cell differences in the relationship between temperature and alkali-metal density. In our experiments, we studied the alkali-metal densities in independent cells using the Faraday rotation method [19], and

TABLE I. Summary of published spin-exchange rate constant measurements and those presented in this paper for various combinations of alkali-metal–^{129}Xe pairs and general experimental conditions. The published measurements are marked by reference numbers, and our present measurements are marked by √.

	K	Rb	Cs
≪1 atm, N_2 dominating	[14]	[14]	[14]
~1 atm, Xe dominating	√	√, [15], [16][a]	√, [17][a]

[a]Reports only the binary collision part of the exchange rate constants.

[1]One amagat $=2.69\times10^{25}$ m^{-3}, which is the number density of ideal gases at 1 atm pressure and 0 °C.

 ©2005 The American Physical Society

fited the experimental results to get empirical formulas specific for our cell conditions. We did not observe the cell to cell differences. Since our results were derived using Faraday measurements, we are free from the possible errors related to using formulas in the literature.

II. THEORY

The alkali-metal–^{129}Xe spin-exchange Hamiltonian [10] is given by

$$V_{\text{alkali-metal–Xe}} = \beta \vec{N} \cdot \vec{S} + \alpha \vec{K} \cdot \vec{S} \tag{1}$$

where $\vec{N}$ is the orbital angular momentum of the two-particle system, $\vec{S}$ is the spin of the alkali-metal valence electron, $\vec{K}$ is the nuclear spin of ^{129}Xe, and α and β are coupling coefficients. The constants α and β depend on various parameters characterizing the relative motion of the interacting particles. The time evolution of the nuclear polarization of ^{129}Xe can be described by the following equation:

$$\frac{d}{dt} P_{\text{Xe}} = (P_{\text{alkali metal}} - P_{\text{Xe}}) \gamma_{SE} - P_{\text{Xe}} \Gamma_{\text{Xe}}, \tag{2}$$

where $P_{\text{alkali metal}}$ is, in the spin-temperature limit [20], the polarization of the valence electrons of alkali-metal atoms, P_{Xe} is the polarization of ^{129}Xe (in the following part, all "Xe" in subscripts will stand for "^{129}Xe" unless otherwise specified), γ_{SE} is the spin-exchange rate between the alkali-metal and ^{129}Xe, and Γ_{Xe} is the relaxation rate of P_{Xe} through mechanisms other than the interaction with alkali-metal atoms. The dominant mechanism contributing to Γ_{Xe} is the wall relaxation. The total relaxation rate for P_{Xe} is $\gamma_{SE}+\Gamma_{\text{Xe}}$.

The term γ_{SE} is proportional to the number density of the alkali metal. Using [ ] to denote the number density of a certain particle, the exchange rate per alkali-metal atom is $\gamma_{SE}/[\text{alkali metal}]$. The spin-exchange rate receives contributions from two different mechanisms, namely, exchange during binary collisions and exchange by forming alkali-metal–^{129}Xe van der Waals molecules [21]. The average breakup rate of the van der Waals molecules depends on the number densities of the particles in the cell. On the other hand, the binary collision part is the velocity-averaged spin-exchange cross section, and is independent of the particle densities.

Under all practical situations, the number density of Xe by far exceeds that of the alkali metal. In the case in which only Xe and alkali-metal vapor are present in the cell, γ_{SE} takes the form [10,15]

$$\gamma_{SE} = [\text{alkali metal}] \left(\frac{\gamma_M \zeta}{[\text{Xe}]} + \langle \sigma v \rangle \right) \tag{3}$$

where $\langle \sigma v \rangle$ is the binary collision term, and γ_M is the molecular spin-exchange term as defined in [15], a constant for any particular alkali-metal–^{129}Xe pair. For our experimental conditions, ζ is a constant solely determined by the relative abundances and nuclear spins of the isotopes for a particular alkali metal (more in Appendix A). Since the natural isotopes of Xe, ^{129}Xe, ^{131}Xe, etc., have the same potential for breaking up van der Waals molecules, [Xe] is taken to be the overall Xe number density.

However, in our experiments and also in most attempts to polarize ^{129}Xe by spin-exchange optical pumping, N_2 is also present in the cell as a buffer gas. The N_2 helps to eliminate the spontaneous emission of photons by excited alkali-metal atoms [22]. Since N_2 and Xe molecules are not equivalent in breaking up the alkali-metal–^{129}Xe molecules, the expression for our γ_{SE} is slightly modified to be

$$\gamma_{SE} = [\text{alkali metal}] \left(\frac{\gamma_M \zeta}{[\text{Xe}] + b[\text{N}_2]} + \langle \sigma v \rangle \right), \tag{4}$$

where b is a constant for each alkali metal, accounting for the difference in the characteristic pressures of N_2 and Xe. The characteristic pressure provides information on the strength of a gas in breaking up the van der Waals molecules [14,15].

III. EXPERIMENT

A. Cell preparation

For all measurements, we used cylindrical Pyrex cells with 1-in. diameter and 3-in. length. Before filling, a cell was attached to a vacuum system, and pumped down while being baked to about 120 °C. After 1–2 days of pumping, the residual pressure in the cell reached $\sim 10^{-7}$ torr. An ampoule previously attached to the cell, containing the alkali metal to be tested (K, Rb, or Cs), was then broken, and the alkali metal was chased using a torch into the cells. Each cell contained a small amount (several milligrams) of alkali metal, sufficient to maintain vapor pressures up to $\sim 10^{20}$ atoms/m^3. The cell was then filled with predetermined amounts of Xe and N_2, while the total pressure was monitored with a hot-ion gauge. Finally the cell was sealed and detached from the system. In an average finished cell, alkali metal presents in the cell wall as tiny droplets, covering less than one-third of the entire cell wall. The cell filling was done at room temperatures, so a scaling factor according to the ideal gas law is used to convert the pressures into number densities in amagats. The overall cell number densities covered the range of 0.2–0.7 amagats. The alkali metals had chemical purities of 99.95%, 99.75%, and 99.98% for K, Rb, and Cs, respectively. For N_2 and Xe, we used research-grade gases with natural isotopic abundances (for N_2, 99.6% ^{14}N; for Xe, 26.4% ^{129}Xe).

B. Experimental setup and procedure

During the experiments, cells were placed in a Teflon oven and heated with hot air. One Ar^+-pumped Ti:sapphire laser provided 4–5 W of output power with a linewidth of $\sim$40 GHz for the $D1$ lines of K and Cs. For the optical pumping of Rb, a diode laser (FAP-system^{TM}) with a fixed 795 nm wavelength, 30 W output, and 550 GHz linewidth was used. The diode laser has an accessorial polarizer producing circularly polarized laser beams, while the output of the Ti:sapphire laser had a linear polarization, and was circularly polarized using an external quarter-wave ($\lambda/4$) plate. The cell temperatures were measured using nonmagnetic re-

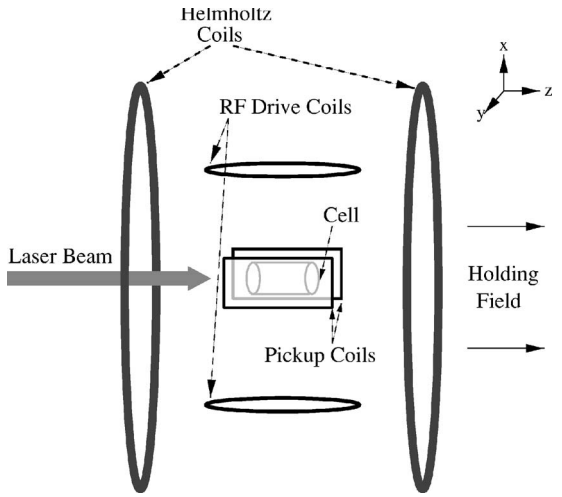

FIG. 1. Experimental setup for the optical pumping and polarization measurement. The oven for heating the cell is not shown. The schematics is not drawn to scale.

sistance temperature detectors placed next to the cells but out of the way of the laser beam. The cell temperatures were in the range of 90 to 170 °C, and were stabilized to be within ±0.4 °C. For K, Rb, and Cs, the temperature ranges are 130–170 °C, 110–150 °C, and 90–130 °C, respectively. The temperature variation along the outer wall of the cell was measured to be smaller than ±1.0 °C. The laser beam covered the cell with good uniformity.

After allowing for approximately 10 min of optical pumping for the ^{129}Xe nuclear polarization to build up and stabilize, adiabatic Fast Passage (AFP) [23] was used to determine the relaxation rate of the polarization of ^{129}Xe, P_{Xe}. A schematic of the setup is shown in Fig. 1. A holding magnetic field (B_0 in the $\hat{z}$ direction) of ~20 G was generated using a pair of 1.4-m-diameter Helmholtz coils. The field inhomogeneities at the center of the coils, where the cells were tested, were measured to be on the order of 10 mG/cm. A second pair of coils, in a direction perpendicular to that of the holding coils, provided the radio-frequency oscillating field for performing AFP. And a third pair of coils, in the third orthogonal direction, picked up the induced resonance signals. The AFP signals at the resonance frequency were separated from the background noises with the help of a lock-in amplifier, and recorded on a PC in text format. The coil system is essentially identical to what was used in the neutron-spin structure function measurements at SLAC [8,24–26]. Two consecutive AFP processes were separated by an interval of at least 4 min, which is ~eight times the relaxation time of the ^{129}Xe polarization.

During the acquisition of each AFP signal, the holding field was swept up past the resonance point, and then back to the initial strength, so that two resonance signals were generated and recorded. After the first resonance, the polarization of ^{129}Xe was reversed, while the polarization of the alkali metal remained unchanged. Being away from its equilibrium value, the ^{129}Xe polarization P_{Xe} underwent a relaxation between the two resonances. Each AFP signal has a Lorentzian shape, and the height of the peak is proportional to the polarization values at the time of resonance. So by

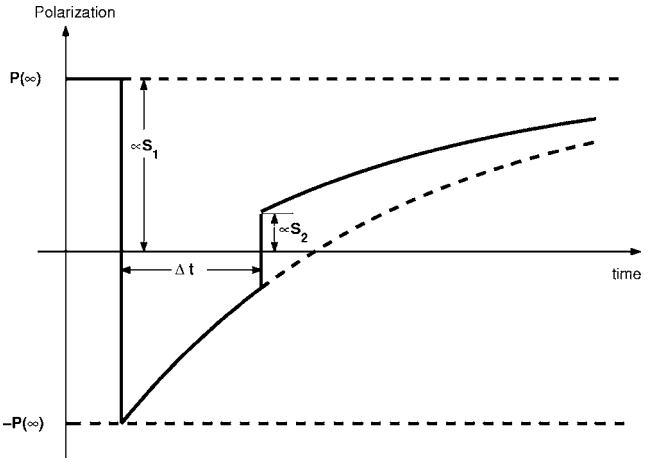

FIG. 2. Polarization development during the AFP process. AFP signals S_1 and S_2 are produced at the points where the polarization is reversed, with the signal sizes proportional to the polarizations at the resonance times. Except for on resonance, P_{Xe} undergoes relaxation toward the equilibrium value $P(\infty)$ with the rate $\gamma_{SE}+\Gamma_{\mathrm{Xe}}$. The ratio S_2/S_1 is determined by the interval between two resonances Δt and by $\gamma_{SE}+\Gamma_{\mathrm{Xe}}$. A small loss of polarization induced by AFP is not explicitly shown in the picture. The laser is on continuously with one helicity state throughout the process.

varying the time interval between the two resonances, and recording the relative ratio of the height of the second peak to that of the first, one calculates the relaxation rate $\gamma_{SE}+\Gamma_{\mathrm{Xe}}$. The time relaxation of P_{Xe} during the AFP process is shown in Fig. 2. Fig. 3 shows a typical AFP signal with two peaks of different heights.

The above approach of measuring $\gamma_{SE}+\Gamma_{\mathrm{Xe}}$ involves only the relative ratio of the two signal sizes (S_1 and S_2 shown in Fig. 2), so any drift of the laser power over time scales larger than ~10 s cancels out. An accurate calibration of the absolute polarization value is also unnecessary. The flips of polarization at the resonance points, however, does introduce a small loss of P_{Xe}, denoted by δ, typically below 5% of the original value. Linear fits of

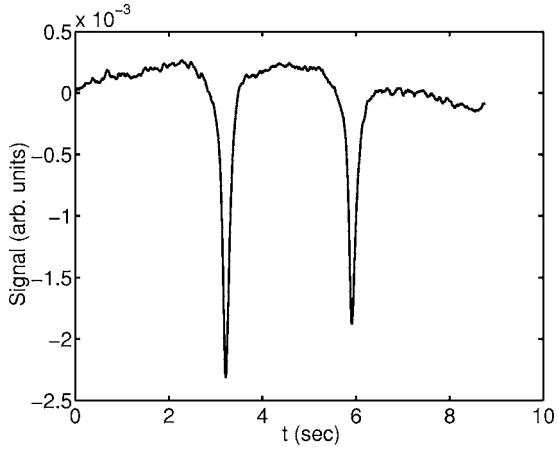

FIG. 3. A typical AFP signal in our tests. The second signal peak has a smaller size than the first due to the relaxation of P_{Xe} between the two resonances. The signal size is in arbitrary units, and roughly corresponds to a 1% ^{129}Xe polarization at equilibrium.

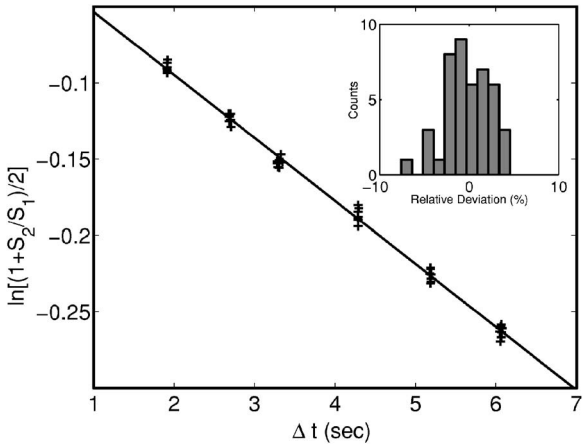

FIG. 4. A linear fit of $\ln[(1+S_2/S_1)/2]$ with respect to Δt for a particular data set. The cell contains 0.124 amagat , 0.248 amagat Xe (natural abundance), and Rb. The quantity $\gamma_{SE}+\Gamma_{Xe}$ is extracted and found to be 0.0413 s^{-1}, while the fitting intercept −0.012 corresponds to the AFP loss of ~2.5%. A histogram, showing the relative deviation of the data points with respect to the fitted line, is plotted as an inset.

$[\ln(1+S_2/S_1)/2]$ with respect to Δt were performed in the data analysis. The fitted slope gives $\gamma_{SE}+\Gamma_{Xe}$, and the intercept gives $\ln(1-\delta/2)$.

IV. RESULTS AND ERROR ANALYSIS

The AFP signal data are recorded, and the two peaks are fitted to Lorentzian shapes using MATLAB. The time intervals between resonances are calculated from the spacings between the peaks and the data sampling frequency of the lock-in amplifier. This time interval ranged from 1 to 9 Small fluctuations of S_1, the size of the first peak, among different data points reflect fluctuations of P_{Xe}, which are mostly due to the slow and small shifts in the laser power and the cell temperature. For a typical data set, the S_1 fluctuations are within ~±7%. In the ratio S_2/S_1, however, most of the uncertainties resulting from the fluctuations cancel out. The linear fit of $\ln[(1+S_2/S_1)/2]$ with respect to Δt for a typical set of data is plotted in Fig. 4. The inset shows a histogram of the relative deviations from the fit of the 44 data points in the data set. The deviations correspond to a ~3%% relative statistical uncertainty.

After the relaxation rate $\gamma_{SE}+\Gamma_{Xe}$ was determined for a cell at a particular temperature, relaxation rates at different temperatures were measured. Different temperatures correspond to different values of the alkali-metal number density. The number densities are calculated from the measured temperatures, using empirical vapor pressure formulas for the three alkali metals. To suit our experimental conditions, we modified the empirical formulas in the literature [27,28] with our direct measurements of alkali-metal densities in independent cells using the Faraday rotation method. The existing formulas in [27,28] are often used in previous measurements, but at least for our condition, these formulas have to be modified by scaling factors, which are 0.32, 0.50, and 0.52, for K, Rb, and Cs respectively. We did not observe any cell-to-cell variation in the relationship between temperature and vapor density. It is worth noting that there are different empirical alkali-metal vapor pressure formulas describing the same temperature-pressure situations. For example, the widely used Killian formula for Rb vapor [27] is different by a factor of 2 from Refs. [29–31], which agree to within a few percent with our Rb measurements. We estimate the relative uncertainty in the alkali-metal densities to be ~10%, which is primarily the uncertainty in the density scaling factors. See Appendix B for more discussion about the Faraday rotation measurements and our complete results for the three alkali metals.

TABLE II. The data of measured relaxation rates tabulated with respect to the measured cell temperature and calculated number density of Cs, for a Cs-Xe cell with 0.093 amagat of N_2 and 0.310 amagat of Xe. The 10% error bars associated with the number densities of Cs are mostly due to the uncertainties in our empirical density formulas.

Temperature (°C)	[Cs] ($(10^{19}$ $m^{-3})$)	$\gamma_{SE}+\Gamma_{Xe}(s^{-1})$
123.7±0.4	2.92±0.29	0.1158±0.0049
110.7±0.4	1.42±0.14	0.0664±0.0037
101.9±0.4	0.853±0.085	0.0479±0.0022
89.9±0.4	0.405±0.040	0.0342±0.0017

The measured relaxation rates are plotted and fitted linearly versus [alkali metal], so that the slope γ_{SE}/[alkali metal] and the intercept Γ_{Xe} can be separated. The quantity γ_{SE}/[alkali metal] has a slight dependence on the temperature, in that the collision term $\langle v\sigma\rangle$ is proportional to $\sqrt{T}$. The experimental temperature ranges span less than 40 °C, which corresponds to ≲5% change in $\langle v\sigma\rangle$, while the alkali-metal density changes drastically with temperature. The wall relaxation rate Γ_{Xe} depends on the average dwelling time of ^{129}Xe at the binding sites on the cell wall, and the average dwelling time depends on cell temperature in

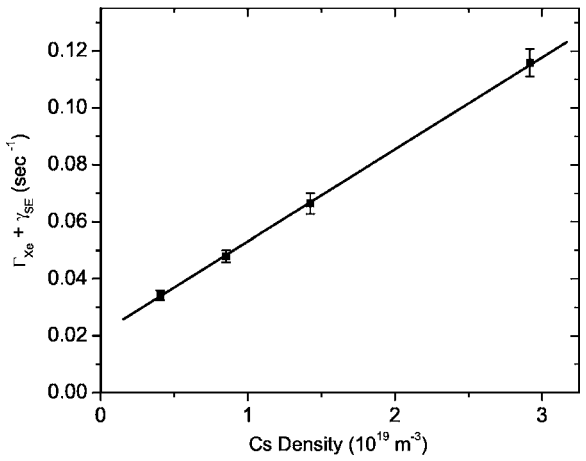

FIG. 5. A linear fit of the measured relaxation rates versus Cs number densities for a Cs-Xe cell with 0.093 amagat. N_2 and 0.310 amagat Xe. Uncertainties along the abscissa are not shown in the plot. The fit gives results for this cell of γ_{SE}/[Cs]=(3.23±0.19) $\times 10^{-21}$ s^{-1} m^3 and Γ_{Xe}=0.0208±0.0020 s^{-1}.

TABLE III. The quantity $\gamma_{SE}/[\mathrm{Cs}]$ measured for the nine Cs-Xe cells, tabulated with the number densities for Xe and N_2 in the cells.

$[\mathrm{Xe}]$ $(10^{24}\ \mathrm{m}^{-3})$	$[N_2](10^{24}\ \mathrm{m}^{-3})$	$\gamma_{SE}/[\mathrm{Cs}](10^{-21}\ \mathrm{m}^3\ \mathrm{s}^{-1})$
12.5	3.33	2.33 2.33±0.10±0.23
5.83	3.33	3.50 3.50±0.10±0.35
3.31	3.33	5.44 5.44±0.19±0.54
8.33	10.0	1.85 1.85±0.10±0.18
8.33	5.00	2.00 2.00±0.12±0.20
8.33	2.50	3.23 3.23±0.19±0.32
4.17	3.33	4.04 4.04±0.13±0.40
4.17	5.00	3.35 3.35±0.08±0.34
4.17	7.50	3.06 3.06±0.08±0.31

the form of $\tau \propto e^{-E_s/kT}$, where E_s is the binding energy [32]. This temperature dependency of Γ_{Xe} also appears to be small compared to that of γ_{SE}, since no notable deviation is observed in the linear fits of $\gamma_{SE}+\Gamma_{\mathrm{Xe}}$ with respect to the alkali-metal density. It has been observed that the wall relaxation rate Γ_{Xe} often decreases when a cell is first heated, and stabilizes after being heated repeatedly. We have applied the "curing" technique [14,16,33], i.e., heated the cell to its highest working temperature several times before actually taking data, to ensure that Γ_{Xe} is constant throughout the measurements, and would not bring extra uncertainty to the final results.

Some representative data for a particular cell (Cs-Xe in this case) and the corresponding fit are shown in Table II and Fig. 5, respectively. For this cell, the temperature range corresponds to a Cs density range of 5×10^{18}–3×10^{19} m^{-3}. In the final results for all three alkali metals, the average temperatures for $\langle v\sigma\rangle$ values are indicated.

As an example, for the $\gamma_{SE}/[\mathrm{Cs}]$ [Cs] values obtained using multiple cells, each with a different ratio between N_2 and Xe densities, we fit these values using Eq. (3), and extract $\gamma_M, \langle\sigma v\rangle$, and b. Table III presents results of $\gamma_{SE}/[\mathrm{Cs}]$ [Cs] for all the Cs cells. The data and fits are plotted in Fig. 6, with the ordinate being $\gamma_{SE}/[\mathrm{Cs}]$ [Cs], and the abscissa being the reciprocal of the effective number density of the cell. The effective number density of the cell is defined as $[\mathrm{Xe}]+b[N_2]$, where b for the Cs-Xe case has the fit value of 0.97. The unit for number densities of Xe and N_2 has been converted from amagats to m^{-3} so that γ_M has the dimension of s^{-1}.

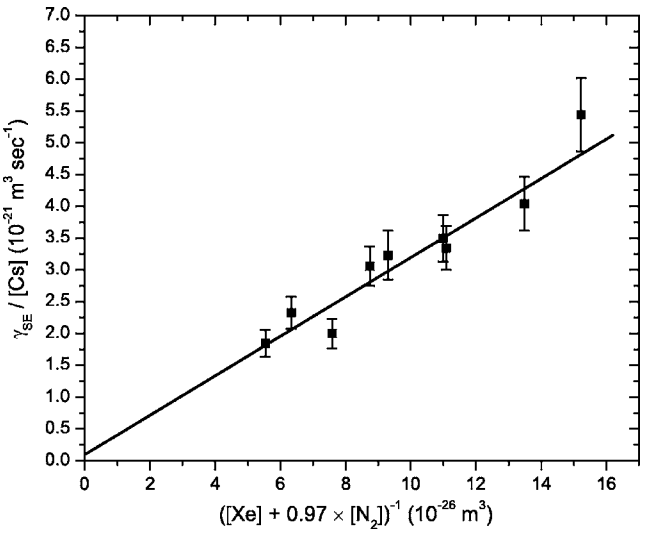

FIG. 6. A plot of $\gamma_{SE}/[\mathrm{Cs}]$ versus the reciprocal of the effective number density in the cells. The effective number density is defined as $[\mathrm{Xe}]+b[N_2]$, where $b=0.97$ for the Cs-Xe case. From the fit, we have $\gamma_{SE}/[\mathrm{Cs}]=9.4\times10^{-23}+(3.1\pm0.4)\times10^4([\mathrm{Xe}]+0.97\times[N_2])^{-1}$ $\mathrm{m}^3\ \mathrm{s}^{-1}$, with the number densities in m^{-3}.

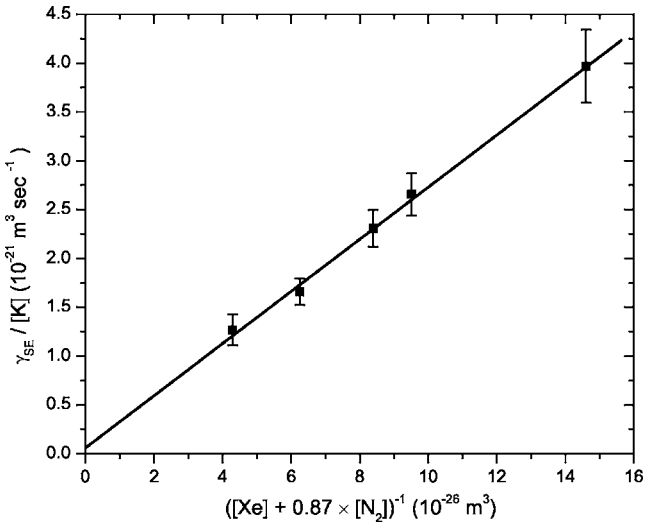

FIG. 7. A plot of $\gamma_{SE}/[\mathrm{K}]$ versus the reciprocal of the effective number density in the cells. From the fitting, $\gamma_{SE}/[\mathrm{K}]=6.3\times10^{-23}+(2.4\pm0.4)\times10^4([\mathrm{Xe}]+0.87\times[N_2])^{-1}$ $\mathrm{m}^3\ \mathrm{s}^{-1}$, with the number densities in m^{-3}.

Studies for the K-^{129}Xe and Rb-^{129}Xe pairs have been similarly performed with five and seven cells, respectively. Raw data were analyzed with the same method, with one minor difference. For Rb we took the value of b, the constant

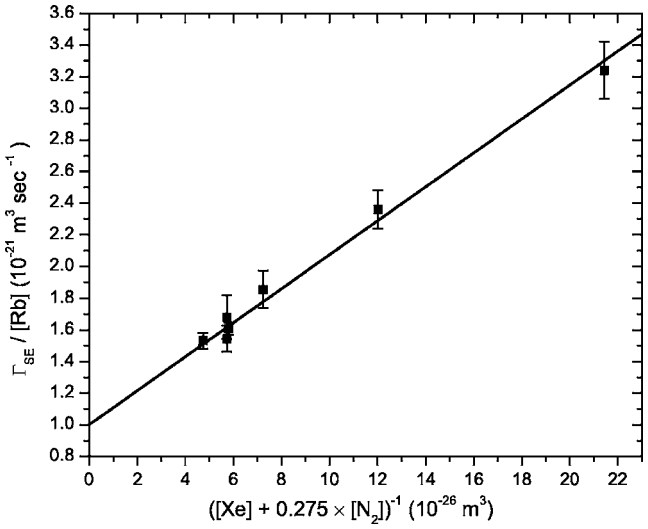

FIG. 8. A plot of $\gamma_{SE}/[\mathrm{Rb}]$ versus the reciprocal of the effective number density in the cells. From the fitting, $\gamma_{SE}/[\mathrm{Rb}]=1.0\times10^{-21}+(9.7\pm1.1)\times10^3([\mathrm{Xe}]+0.275\times[N_2])^{-1}$ $\mathrm{m}^3\ \mathrm{s}^{-1}$, with the number densities in m^{-3}.

TABLE IV. Experimental results for $\langle v\sigma\rangle$, γ_M, and b for the three alkali metals. The ζ values are calculated from the relative abundances and nuclear spins of the alkali metals' isotopes. The first term in the uncertainties of the γ_M values comes from statistical scatterings of the data points, and the second term is the systematic uncertainty.

Alkali metal	$\langle v\sigma\rangle$ (10^{-22} m^3 s^{-1})	ζ (calculated)	γ_M (10^5 s^{-1})	b
K	0.63	0.125	1.92 1.92±0.24±0.20	0.87
Rb	10	0.095	1.02 1.02±0.08±0.09	0.275
Cs	0.94	0.0625	4.92 4.92±0.63±0.49	0.97

for in the effective number density, from calculations by Cates *et al.* [15]. The fittings for K and Rb are shown in Figs. 7 and 8. The results for the three alkali-metal–pairs are listed in Table IV. Since all of the test cells contain overall number densities (Xe and) under 1 amagat, the data points are not close enough to the high-density limit to give a very accurate fit value for the intercept, or the binary collision term $\langle v\sigma\rangle$. The results for $\langle v\sigma\rangle$ are, therefore, only rough estimates. The uncertainties on the $\langle v\sigma\rangle$ values are large and have not been marked. The γ_M results have higher precision. Due to the limited number of data points, the results for b tend to have large uncertainties too, estimated to be on the order of 50% relative. The fact that the two fitted values of b (for K and Cs) are about three times larger than that of Rb, which was taken from existing literature, may be an indication of this large uncertainty.

As previously discussed, the $\langle v\sigma\rangle$ values have slight temperature dependencies, and the results listed in Table IV for K, Rb, and Cs are for average temperatures of 150, 130, and 110 °C, respectively.

As stated earlier, the major systematic uncertainty comes from the determination of alkali-metal densities, which we estimate to be a ~10% relative uncertainty. Other uncertainties (e.g., the knowledge of the pressures of the gases during fillings) do not exceed ~3%. An overall 10% systematic uncertainty has been included in Table IV.

V. SUMMARY AND DISCUSSION

We have found the experimental values for $\langle v\sigma\rangle$, γ_M, and b, characterizing the alkali-metal–spin-exchange interactions for three alkalis metals Rb, K, and Cs. Compared with previous measurements of $\langle v\sigma\rangle$ for the Rb-^{129}Xe pair [15,16,34],[2] which give

$$\langle v\sigma\rangle = (3.70 \pm 0.15 \pm 0.55) \times 10^{-22}\ \mathrm{m^3\ s^{-1}}$$

and

$$\langle v\sigma\rangle = (2.18 \pm 0.12) \times 10^{-22}\ \mathrm{m^3\ s^{-1}},$$

respectively, our result 1.0×10^{-21} m^3 s^{-1} is different, in the latter case by a factor of 4. For Cs, Jau *et al.* [17] reported

$$\langle v\sigma\rangle = (4.1 \pm 0.3) \times 10^{-22}\ \mathrm{m^3\ s^{-1}},$$

which is a factor of 2 smaller than our value. Part of the difference may come from the fact that our measurements were performed at low magnetic field (~20 G), while the values reported by [16,34] and [17] were measured at high magnetic field (~9 T) Tesla, and then extrapolated to the low-field condition. Also, our values of $\langle v\sigma\rangle$ have large uncertainties, because they are intercepts of the linear fits.

On the other hand, our γ_M results, being the slope of the fits, have high precision. Although our γ_M value for Rb-Xe pair $(10.2\pm0.8\pm0.9)\times10^4$ s^{-1} is about three times as large as the result from measurements by Cates *et al.* [15], which is

$$\gamma_M = (2.92 \pm 0.18 \pm 0.41) \times 10^4\ \mathrm{s^{-1}},$$

some of the difference maybe due to the Killian empirical formula which was used to calculate the Rb density in Ref. [15], while our direct measurements of the Rb density suggest an empirical formula giving about half the value of the Killian formula.

The γ_M values for K and Cs have not been previously measured at high Xe density (i.e., ~1 amagat).

Presently most methods [1,2,7,35] employing ^{129}Xe polarization by spin exchange with alkali metals used total number densities of Xe and $N_2 \lesssim 1$ amagat, similar to our conditions. For such cell densities, it is the van der Waals mechanism that dominates the spin-exchange process, and our precise determinations of γ_M's are helpful additions to these cases. Also, the N_2 density is usually one order of magnitude lower than the Xe density, so the uncertainties in b do not lead to significant errors in estimates of spin-exchange rates either. Nonetheless, it is desirable to complement our studies with tests in the high-density limit as has been done for Rb-^{129}Xe by Jau *et al.* [16,34]. Such measurements can provide better determinations for $\langle v\sigma\rangle$ values. More tests similar to these presented in this paper can help to determine b values better.

Since different alkali metals have different values for ζ and b, their γ_M's cannot be directly compared. But comparisons might be done by calculating the spin-exchange rates for different alkali metals under typical conditions, so that we can gain insight into the choice of the most promising alkali metal for polarizing ^{129}Xe. An example of such comparisons is shown in Table V, in which the number densities for Xe and N_2 are taken to be 0.35 amagat and 0.15 amagat,

[2]The original measurements in [16] are for high magnetic fields (~9 T); a "zero field extrapolation" was reported in [34] which gives the quoted value.

TABLE V. Comparison of spin-exchange rates under a typical condition for the three alkali metals K, Rb, and Cs. This condition has [Xe]=0.35 amagat and $[N_2]$=0.15 amagat; [alkali metal] is set at 2.5×10^{19} atoms/m^3, the corresponding temperatures for different alkali metals (calculated from our empirical alkali-metal density formulas) are listed in the table.

Alkali metal	Spin-exchange rate (sec^{-1})	Corresponding temperature (°C)
K	0.031	164
Rb	0.048	136
Cs	0.062	122

respectively. The number density for the alkali metal is set at 2.5×10^{19} atoms/m^3, which corresponds to different temperatures for different alkali metals, as shown in Table V. Naturally, laser availability, pumping efficiency, temperature to maintain sufficient alkali-metal number density, and many other issues should also be considered for making such a choice.

In summary, we have made measurements for the spin-exchange rates between alkali-metal–^{129}Xe pairs for three alkali metals K, Rb, and Cs, under low magnetic field (~20 G) and with cell densities in the range of 0.2 to 0.7 amagat. The two terms in the spin-exchange rate, the binary collision term and the van der Waals molecular term, have been separated by studying the cell density dependence of the spin-exchange rates. The constants that govern the spin-exchange process, γ_M, $\langle v\sigma\rangle$, and b, have been determined. These results, especially the value of γ_M, provide useful information for estimating the spin-exchange rates in the three alkali-metal ^{129}Xe pairs under typical polarizing conditions, and ultimately for achieving optimal polarizations for hyperpolarized ^{129}Xe in this density range.

ACKNOWLEDAMENT

This work was supported by the National Science Foundation under Grant No. PHY-0244245.

APPENDIX A: CALCULATION OF ζ

Under the short-molecular-lifetime limit [10,15], which is always satisfied for our experimental conditions, ζ takes the form of [15]

$$\zeta=\sum_{\text{isotopes}}\frac{(\text{fraction of isotope})\times\langle\hat{F}^2-F_z^2\rangle}{(2I+1)^2}. \quad \text{(A1)}$$

Unlike in the case of Ref. [15], where the alkali-metal polarization is approximately zero, for our case the alkali-metal polarization is almost 100%. Under this limit,

$$\langle F^2-F_z^2\rangle=\left(I+\frac{1}{2}\right),$$

$$\zeta=\sum_i\frac{f_i}{4I_i+2}. \quad \text{(A2)}$$

Here f_i is the relative abundance of the ith isotope, and I_i is the nuclear spin of that isotope.

For Rb, there are two isotopes ^{85}Rb and ^{87}Rb with nuclear spins 5/2 and 3/2, respectively, and abundances 0.7215 and 0.2785. For our conditions this yields ζ=0.095. For K, the two most abundant isotopes ^{39}K and ^{41}K both have nuclear spin 3/2 , so ζ=0.125. For Cs, whose only natural isotope is ^{133}Cs with nuclear spin 7/2, ζ=0.0625.

APPENDIX B: DIRECT MEASUREMENTS OF THE ALKALI-METAL NUMBER DENSITY USING FARADAY ROTATION METHOD

We used the Faraday rotation method [19,36] to measure the alkali-metal number density in the cells. When linearly polarized light with frequency close to absorption lines of the alkali metal passes through the alkali-metal vapor with magnetic field in the direction of the light, the light's polarization plane gets rotated by an angle proportional to the number density of the alkali metal. We used laser light close to the $D1$ lines of the alkali metals (within ±0.3 nm of the lines); after ignoring the higher-order corrections, the rotation angle is approximately given by

$$\Delta\theta=\frac{2[\text{alkali metal}]L\lambda_0^4 r_e\mu_B B/h}{9c(\lambda-\lambda_0)^2} \quad \text{(B1)}$$

where L is the length of the cell through which the laser passes, λ is the wavelength of the laser, λ_0 is the resonant wavelength, r_e is the classical electron radius, μ_B is the Bohr magneton, h is the Planck constant, and c is the speed of light. We have approximated the oscillator strength of the $D1$ lines to be $\frac{1}{3}$. In the equation only the leading term has been retained, but for the detuning we used $0.05<|\lambda-\lambda_0|>0.3$ nm; the resulting systematic error has been estimated to be less than 3%.

In our experiments, we used a Ti:sapphire laser beam with power ~300 mW , and a magnetic field ~±40 G. Define the direction of the light's propagation and the magnetic field to be $\hat{z}$. The laser beam first passes through a polarizing beam splitter cube to ensure a pure linear polarization, then through the sample cell; after emerging from the cell, the electric field of the light can be assumed to have the form of $\vec{E}=E_0(\cos\theta\hat{x}+\sin\theta\hat{y})\cos(\omega t)$ where θ is with respect to the horizontal polarization direction ($\hat{x}$), and ω is the laser frequency. The beam then goes through a photoelastic modulator whose modulator axis is on the vertical direction ($\hat{y}$), so that the phase difference between the two polarization directions is modulated by $\psi(t)=\psi_0\cos(\omega_1 t)$, where ω_1 is the modulating frequency and ψ_0 is the maximum modulating angle. After that, the beam passes a second polarizing beam splitter cube whose axis is at 45° with the horizontal direction and is finally detected by a photodiode. The photodiode signal can be calculated to have the form of

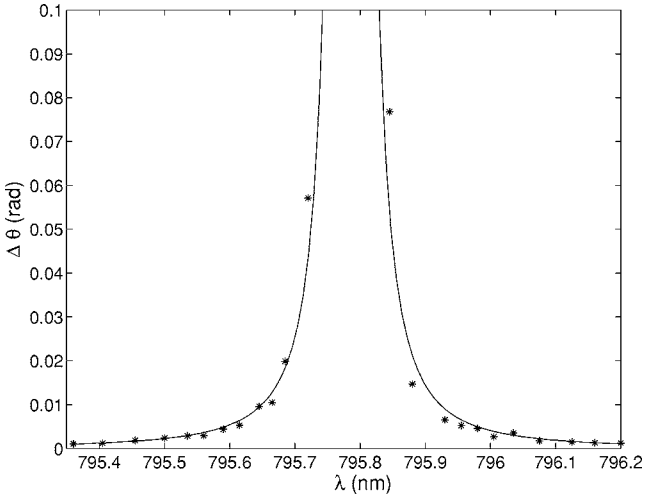

FIG. 9. A typical fit of the Faraday rotation angle with respect to the wavelength of the incident light in our density measurement. This fit is for a Rb cell, and indicates a Rb density of 2.53 $\times 10^{19}$ m^{-3}.

$$I \propto \frac{E_0^2}{4}\{1 + \sin(2\theta)\cos[\psi(t)]\}. \tag{B2}$$

Expand the $\cos(\psi)$ term into components with frequencies ω_1, $2\omega_1$, …, and keep only the lowest-order terms; now

$$I \approx \text{const} \times [1 + J_0(\psi_0)\sin 2\theta - 2\sin 2\theta J_2(\psi_0)\cos(2\omega_1 t)] \tag{B3}$$

where J_n are Bessel functions of the first kind. We have assumed that the circular polarization of the laser resulting from the circular dichroism of the alkali-metal vapor is negligible, which we have verified by monitoring the component of I with frequency ω_1.

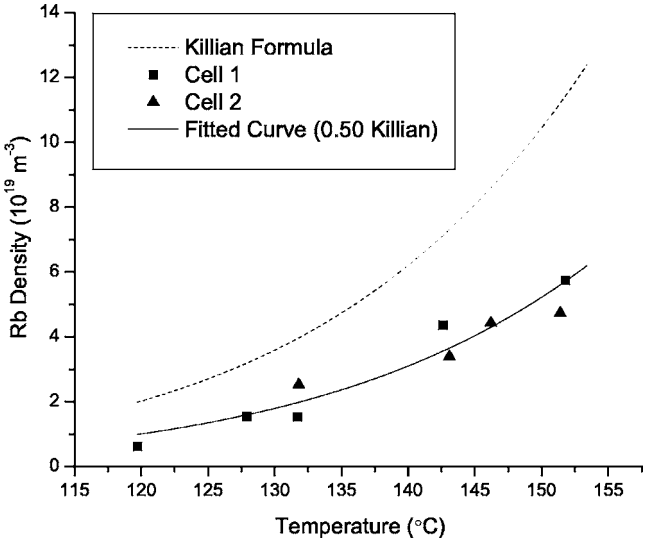

FIG. 10. The Rb densities from our direct measurements, together with Killian's empirical density formula and the modified Killian formula we fitted from our data.

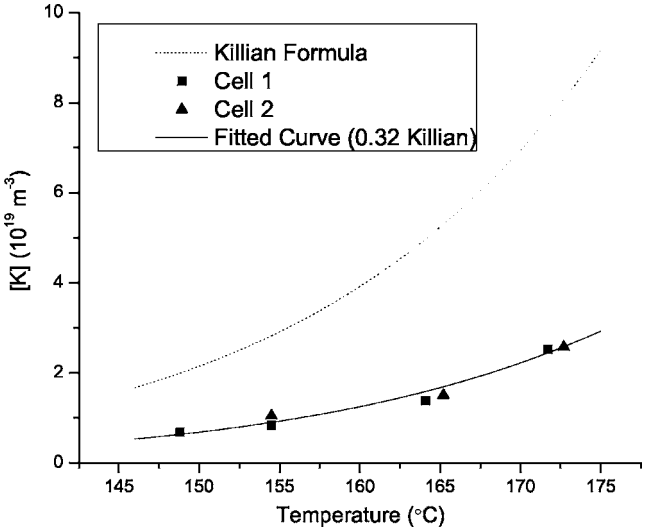

FIG. 11. The K densities from our direct measurements, together with Killian's empirical density formula and the modified Killian formula we fitted from our data.

By choosing $\psi_0 = 2.406$ rad rad, we can set $J_0(\psi_0) = 0$, so that the dc component of I is independent of θ. A lock-in amplifier is used to separate the $2\omega_1$ component. So now

$$|I_{2\omega_1}/I_{dc}| = |2J_2(\psi_0)\sin(2\theta)|. \tag{B4}$$

We recorded different values of θ at two different magnetic fields ($\sim +40$ and ~ -40 G,), so their difference is proportional to the alkali-metal density and inversely proportional to the square of the wavelength detuning $((\lambda - \lambda_0)$,

$$\Delta\theta = \left(\frac{2L\lambda_0^4 r_e \mu_B \Delta B}{9ch}\right)[\text{alkali metal}]/(\lambda - \lambda_0)^2. \tag{B5}$$

We then varied the laser wavelength λ within ± 0.3 nm of λ_0, and recorded $\Delta\theta$ as a function of λ; fitting the data to Eq.

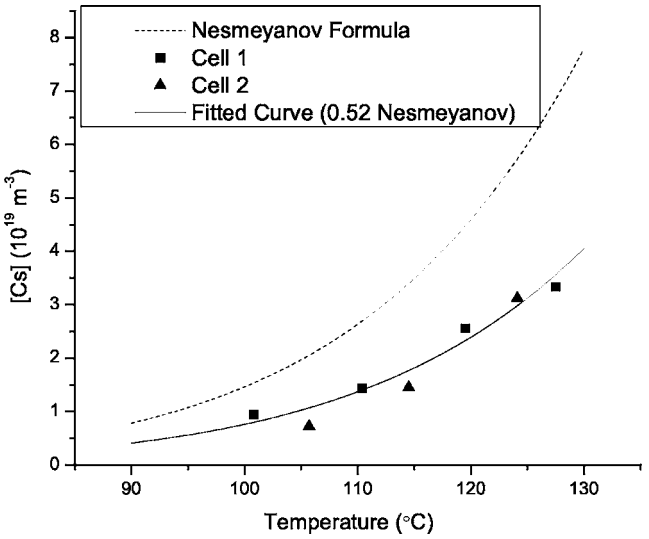

FIG. 12. The Cs densities from our direct measurements, together with Nesmeyanov's empirical density formula and the modified formula we fitted from our data.

(B5), the alkali-metal density can be readily calculated. Figure 9 shows a typical fit, which corresponds to a Rb density of 2.53×10^{19} m^{-3}.

For each alkali metal, we made measurements for two independent cells (i.e., not made from the same glass manifold) and at different temperatures. The temperature measurement was done in the same manner as for our exchange constant measurements, which has been described in Sec. III; therefore the possible systematic uncertainty in the temperature measurement would not be carried into the determination of alkali-metal density. For K, Rb, and Cs, we have plotted our measurements along with the empirical formulas from refs. [27,28] in Figs. 10, 11, and 12. We did not observe any significant cell-to-cell variation in the alkali-metal vapor densities. A preliminary conjecture about the alkali-metal vapor density is that it can be vastly changed by contaminants in the alkali metals. So the densities in our cells were different from the values from existing formulas, but did not significantly differ among themselves because all our cells were made in the same manner using alkali metals with the same specifications.

Since the cell-to-cell variations in alkali-metal densities were absent in our cells, we could use our Faraday rotation measurements to fit empirical density formulas specific for our case. We have assumed that the formulas that would suit our experimental conditions would differ from the empirical formulas only by scaling factors, and fitted our data to estimate these factors, as indicated in the plots. These modified formulas we obtained are

$$[\mathrm{K}] = 10^{10.34-4964/T}/kT, \tag{B6}$$

$$[\mathrm{Rb}] = 10^{9.25-4132/T}/kT, \tag{B7}$$

$$[\mathrm{Cs}] = 10^{12.89-4041/T}/T^{1.35}/kT, \tag{B8}$$

where the unit for all number densities is m^{-3}, and the unit for T is K.

Based on the fitted curves, we estimate the uncertainty in the number densities we calculated from our modified formulas to be 10%.

[1] B. Driehuys, G. D. Cates, E. Miron, K. Sauer, D. K. Walter, and W. Happer, Appl. Phys. Lett. **69**, 1668 (1996).

[2] W. Shao, G. Wang, R. Fuzesy, E. W. Hughes, B. A. Chronik, G. C. Scott, S. M. Conolly, and A. Macovski, Appl. Phys. Lett. **80**, 2032 (2002).

[3] M. S. Albert, G. D. Cates, B. Driehuys, W. Happer, B. Saam, C. S. Springer, and A. Wishnia, Nature (London) **370**, 188 (1994).

[4] Y. Q. Song, B. M. Goodson, and A. Pines, Spectroscopy (Eugene, Or.) **14**, 26 (1999).

[5] D. Raftery, H. Long, T. Meersmann, P. J. Grandinetti, L. Reven, and A. Pines, Phys. Rev. Lett. **66**, 584 (1991).

[6] J. P. Butler, R. W. Mair, D. Hoffmann, M. I. Hrovat, R. A. Rogers, G. P. Topulos, R. L. Walsworth, and S. Patz, J. Phys.: Condens. Matter **14**, L297 (2002).

[7] M. V. Romalis and M. P. Ledbetter, Phys. Rev. Lett. **87**, 067601 (2001).

[8] P. L. Anthony *et al.*, Phys. Rev. Lett. **71**, 959 (1993).

[9] A. B. Baranga, S. Appelt, M. V. Romalis, C. J. Erickson, A. R. Young, G. D. Cates, and W. Happer, Phys. Rev. Lett. **80**, 2801 (1998).

[10] W. Happer, E. Miron, S. Schaefer, D. Schreiber, W. A. van Wijngaarden, and X. Zeng, Phys. Rev. A **29**, 3092 (1984).

[11] S. Appelt, A. B. Baranga, C. J. Erickson, M. V. Romalis, A. R. Young, and W. Happer, Phys. Rev. A **58**, 1412 (1998).

[12] J. Luo, X. Mao, J. Chen, S. Wang, M. Zhao, L. Fu, and X. Zeng, Appl. Magn. Reson. **17**, 587 (1999).

[13] C. H. Volk, T. M. Kwon, and J. G. Mark, Phys. Rev. A **21**, 1549 (1980).

[14] X. Zeng, Z. Wu, T. Call, E. Miron, D. Schreiber, and W. Happer, Phys. Rev. A **31**, 260 (1985).

[15] G. D. Cates, R. J. Fitzgerald, A. S. Barton, P. Bogorad, M. Gatzke, N. R. Newbury, and B. Saam, Phys. Rev. A **45**, 4631 (1992).

[16] Y. Y. Jau, N. N. Kuzma, and W. Happer, Phys. Rev. A **66**, 052710 (2002).

[17] Y. Y. Jau, N. N. Kuzma, and W. Happer, Phys. Rev. A **69**, 061401(R) (2004).

[18] B. Chann, E. Babcock, L. W. Anderson, and T. G. Walker, Phys. Rev. A **66**, 032703 (2002).

[19] Z. Wu, M. Kitano, W. Happer, M. Hou, and J. Daniels, Appl. Opt. **25**, 4483 (1986).

[20] L. W. Anderson, F. M. Pipkin, and J. C. Baird, Phys. Rev. **120**, 1279 (1960).

[21] M. A. Bouchiat, J. Brossel, and L. C. Pottier, J. Chem. Phys. **56**, 3703 (1972)

[22] Thad G. Walker and William Happer, Rev. Mod. Phys. **69**, 629 (1997).

[23] A. Abragam, *The Principles of Nuclear Magnetism* (Oxford University Press, Oxford, England, 1961).

[24] J. R. Johnson *et al.*, Nucl. Instrum. Methods Phys. Res. A **356**, 148 (1995).

[25] H. L. Middleton, Ph.D. thesis, Princeton University, 1994 (unpublished).

[26] M. V. Romalis, Ph.D. thesis, Princeton University, 1994 (unpublished).

[27] T. J. Killian, Phys. Rev. **27**, 578 (1926).

[28] A. N. Nesmeyanov, *Vapor Pressure of the Elements* (Academic, New York, 1963).

[29] R. Hultgren *et al.*, *Selected Values of the Thermodynamic Properties of the Elements* (American Society for Metals, Materials Park, OH, 1973).

[30] C. J. Smithells, *Metals Reference Handbook*, 7th ed. (Butterworths, London, 1955).

[31] D. H. Scott, Philos. Mag. **47**, 32 (1924).

[32] B. Driehuys, G. D. Cates, and W. Happer, Phys. Rev. Lett. **74**, 4943 (1995).

[33] Z. Wu, W. Happer, M. Kitano, and J. Daniels, Phys. Rev. A **42**, 2774 (1990).

[34] Y. Y. Jau, N. N. Kuzma, and W. Happer, Phys. Rev. A **67**, 022720 (2003).

[35] A. Wong-Foy, S. Saxena, A. J. Moule, H. M. L. Bitter, J. A. Seeley, R. McDermott, J. Clarke, and A. Pines, J. Magn. Reson. **157**, 235 (2002).

[36] E. Vliegen, S. Kadlecek, L. W. Anderson, T. G. Walker, C. J. Erickson, and W. Happer, Nucl. Instrum. Methods Phys. Res. A **460**, 444 (2000).